Numerical Simulation of Heat and Mass transfer in Stagnation point flow of Casson Nanofluid over a Porous Stretching sheet with Thermal Radiation.

Kapil kumar[1,*], Bhupander Singh[1], Pravendra Kumar[1], Rahul Kumar[1]

[1] *Department of Mathematics, Meerut College, Meerut, U.P.-250002*

Abstract

This research article introduces an examination of heat and mass transfer in the stagnation point flow of MHD Casson nanofluid across stretching sheet within a porous medium. The study involves the transformation of a set of non-linear partial differential equations (PDEs) governing fluid flow into a set of ordinary differential equations (ODEs) through the use of similarity transformations and non-dimensional variables. These equations are subsequently solved numerically utilizing the bvp4c functionality within the MATLAB software. The study investigates the effect of different key parameters such as Casson fluid parameter, porosity parameter, magnetic parameter, stagnation point parameter, thermal radiation parameter, Prandtl number, Brownian motion parameter, thermophoresis parameter, and Lewis number on the velocity, temperature, and concentration profiles, which are illustrated and analyzed graphically.

Keywords: Nanofluid, Casson fluid, Stretching sheet, Magnetohydrodynamics, Thermal Radiation, Porous medium

1. Introduction

A fundamental challenge within field of fluid dynamics pertains to the analysis of viscous boundary layer flow of incompressible fluids across stretched sheet due to stagnation point flow. Hiemenz was the pioneer in investigating two-dimensional flow of fluid at stagnation point along surface [1], marking the initial exploration of this phenomenon. Subsequently, researchers have expanded the scope of stagnation point flow analysis to encompass various fluid properties and physical factors. The applications of studying flow across a surface at a boundary layer stagnation point, particularly in context of fluids that is non-Newtonian, have attracted significant attention from industries involved in polymer processing, biological processes, environmental remediation, aerodynamic plastic sheet extrusion, production of glass fibers within a liquid film boundary layer, condensation processes, as well as the cooling and drying processes of paper and textiles. Moreover, sectors such as metallurgy and petroleum extraction exemplify the numerous industrial domains where analyzing Heat transport is extremely important in non-Newtonian fluids. Sakiadis [2] conducted pioneering study of stretching sheet's effects on boundary layer flow on a continuously extending surface moving at a constant velocity. Building upon Sakiadis's work, Tsou et al. [3] furthered the investigation by exploring transfer of heat within boundary layer on uniformly moving surface.

Magnetohydrodynamic (MHD) flow represents a significantly crucial area of study because of its broad scope implications in various industrial procseess. These processes encompass the handling of magnetic materials, the refining of crude oil, the generation of MHD electrical power, the fabrication of glass, geophysics applications, and the production of paper, all of which rely on the influence of magnetic field on the viscous behavior of electrically conductive fluid. Ghazwani et al. [4] delved into the utilization of nanoparticles in magnetohydrodynamics flow at a stagnation point over a surface that can deform, considering the effects of porosity and boundary slip phenomena. Expanding on this, Ali et al. [5] explored nonlinear stretchable surface with MHD nanofluid flow while considering diverse factors such as Joule heating, thermal radiation, fluctuating fluid viscosity, and viscous dissipation, alongside the existence of electric field. Furthermore, to scrutinize impacts of magnetic field, thermal radiation, and chemical reactions on fluid flow and transmission of heat within boundary layers of nanofluids over stretching surface that is not isothermal via a porous medium, Awati et al. [6] embarked on a comprehensive analysis. This extensive research contributes significantly to the understanding and advancement of magnetohydrodynamics and its applications across various industrial sectors, paving the way for enhanced efficiency and innovation in related processes. Waqas et al.'s [7] three-dimensional study of the mass and heat transfer characteristics of hybrid nanofluid, along with electro-magneto hydrodynamics, was aimed at improving heat transmission. Viscosity dissipation of an exponentially extending sheet and internal heat production in Casson MHD nanofluid flow were explored numerically by Kemparaju et al. [8].

Common fluids like water and ethylene glycol, for example, have their thermal conductivity improved by mixing metal or metallic oxide nanoparticles with a base fluid to speed up heat transfer by improving the nanofluid's thermal transport. This

*Corresponding author

Email address: kapiltomadia071993@gmail.com (Kapil kumar)

can be attributed to the nanoparticles' increased heat conductivity and the corresponding Brownian motion. Stable nanoparticle suspensions in base fluids are known as nanofluids, which exhibit enhanced thermophysical characteristics relative to base fluid [9]. Nanofluids have been used in various industries, including solar panels and CO2 absorption [10]. In the oil and gas industry, nano-emulsions with adjustable density have been used as cleaning fluids to remove sludge from well walls [11]. The addition of nanoparticles to fluids creates smart fluids, which have enhanced properties that depend on nanoparticle dimensions. These nanofluids have advantages such as increased sedimentation stability and improved thermal, optical, stressstrain, electrical, and rheological properties. Thermal radiation has been investigated in several papers. Fu Gui et al. [12] conducted a study on the influence of thermal radiation on flow characteristics of nanofluid and transfer of heat across porous stretching/shrinking surface subjected to an angled magnetic field. The research delved into the intricate interactions between thermal radiation, nanofluid flow, and heat transfer phenomena. Reddy et al. [13] investigated the impacts of magnetic field on unsteady magnetohydrodynamic (MHD) flow of water-based nanofluid coupled with radiative heat transfer. The investigation shed light on the complexities arising from the combined influence of magnetic fields and nanofluid dynamics on heat transfer processes. Asghar et al. [14] statistically analyzed effect of heat radiation on the rotational flow behavior of a hybrid nanofluid in three dimensions. The study provided valuable insights into the heat transfer mechanisms in complex fluid flow scenarios. Bhupendra K. et al. [15] investigated the effects of mass transfer, heat transmission, and entropy generation in the flow of Jeffrey fluid under the influence of solar light, copper nanoparticles, and gyrotactic bacteria. The research highlighted the multifaceted nature of transfer of heat and mass processes in bio-nanofluid systems. Neha et al. [16] computationally analized the thermally radiative hybrid nanofluid incompressible flow generated by a revolving disk that is stretchable radially. The investigation aimed to understand the intricate interplay between thermal radiation, fluid flow, and rotating disk dynamics in nanofluid systems.

Casson nanofluid is a type of nanofluid that has been extensively studied in various research papers. It is known for its excellent heat transfer rates and has numerous applications in medical and industrial fields [17]. The behavior of Casson nanofluid has been investigated in different scenarios, such as in a porous medium [18], in presence of swimming motile organisms [19], and under influence of an applied changing magnetic flux [20]. Mathematical models and numerical methods have been used to analyze the flow and thermal/mass transfer characteristics of Casson nanofluid [21] . The effects of various parameters, such as viscosity, conductivity, Darcy parameter, and magnetic field, have been studied to understand the behavior of Casson nanofluid . Overall, the research on Casson nanofluid provides valuable insights into its properties and potential applications in different fields. Within the realm of comprehensive nanofluid studies, scholars seeking insightful research can turn to specific references outlined in the works [[22],[23],[24], [25], [26], [27], [28],[29], [30]].

2. Problem Formultion

In the current mathematical model, we examine a two-dimensional steady MHD state stagnation point flow of Casson nanofluid across a porous stretching sheet. The setup of the coordinate system, x-axis is positioned along the sheet's surface and y-axis perpendicular to it. The flow takes place in the region where $y \geq 0$. At infinity, the ambient values of T_∞ and C_∞ are used for T and C, independently. The distribution of the free-stream velocity is considered to be assumed in the form of $U_\infty = ax$, where $u_w = bx$ signifies the velocity of the stretching sheet, with a and b as positive constants. The equations for steady, laminar Casson nanofluid's boundary layer flow passing across stretchable sheet, incorporating boundary layer approximation, include expressions for mass, momentum, thermal energy, and concentration.

$$\frac{\partial u}{\partial x} + \frac{\partial v}{\partial y} = 0 \tag{1}$$

$$u\frac{\partial u}{\partial x} + v\frac{\partial v}{\partial y} = U_\infty \frac{\partial U_\infty}{\partial x} + \nu\left(1 + \frac{1}{\beta}\right)\frac{\partial^2 u}{\partial y^2} - \frac{\nu}{\kappa_1}(u - U_\infty) - \frac{\sigma B_0^2}{\rho}(u - U_\infty) \tag{2}$$

$$u\frac{\partial T}{\partial x} + v\frac{\partial T}{\partial y} = \alpha\frac{\partial^2 T}{\partial y^2} + \frac{(\rho C_p)_p}{(\rho C_p)_f}\left[D_B\frac{\partial T}{\partial y}\frac{\partial C}{\partial y} + \frac{D_T}{T_\infty}\left(\frac{\partial T}{\partial y}\right)^2\right] - \frac{1}{\rho C_p}\frac{\partial q_r}{\partial y} \tag{3}$$

$$u\frac{\partial C}{\partial x} + v\frac{\partial C}{\partial y} = D_B\frac{\partial^2 C}{\partial y^2} + \frac{D_T}{T_\infty}\frac{\partial^2 T}{\partial y^2} \tag{4}$$

The specific boundary conditions for the problem are outlined as follows:

$$u = u_w = bx,\ v = 0,\ T = T_w,\ C = C_w \ \text{ at } \ y = 0 \tag{5}$$

$$u = U_\infty = ax,\ C = C_\infty,\ T = T_\infty \ \ as \ \ y \to \infty \tag{6}$$

The quantities u and v represent velocity components of Jeffery nanofluid in x and y directions, respectively. In energy boundary layer equation (3), radiative heat flux q_r is estimated using the Rosseland approximation [31] for thermal radiation, which is expressed as follows:

$$q_r = -\frac{4}{3}\frac{\sigma^*}{k^*}\frac{\partial T^4}{\partial y} \tag{7}$$

Whereas σ^* = Stephan Boltzmann constant, k^* = Rosseland mean spectral absorption coefficient.

Through a Taylor series expansion centered at the ambient temperature T_∞, it becomes apparent that the term T^4 can be treated as a linear relationship with temperature. This simplification is attained by disregarding higher-order terms in the approximation process.

$$T^4 \approx 4T_\infty^3 T - 3T_\infty^4 \tag{8}$$

Utilizing Equations (7) and (8), we derive the following:

$$\frac{\partial q_r}{\partial y} = -\frac{16}{3}\frac{\sigma^* T_\infty^3}{k^*}\frac{\partial^2 T}{\partial y^2} \tag{9}$$

The problem's analysis is made simpler through the use of the subsequent similarity transformation:

$$\psi = \sqrt{b\nu}xf(\eta), \quad \eta = y\sqrt{\frac{b}{\nu}}$$
$$\theta(\eta) = \frac{T - T_\infty}{T_f - T_\infty}, \ \phi(\eta) = \frac{C - C_\infty}{C_\infty} \tag{10}$$

where $\psi(x, y)$ represent stream function and is defined as,

$$u = \frac{\partial \psi}{\partial y}, \quad v = -\frac{\partial \psi}{\partial x} \tag{11}$$

Equations (1) satisfy identically and equations (2), (3), and (4) are reduced to the following set of nonlinear ODE's with the help of the similarity transformation described above.

$$\left(1 + \frac{1}{\beta}\right) f'''(\eta) - (f'(\eta))^2 + f(\eta)f''(\eta) + (M + K)(r - f'(\eta)) + r^2 = 0 \tag{12}$$

$$(1 + Nr)\theta''(\eta) + Pr[\theta'(\eta)f(\eta) + N_b\theta'(\eta)\phi'(\eta) + N_t(\theta'(\eta))^2] = 0 \tag{13}$$

$$\phi''(\eta) + LePrf(\eta)\phi'(\eta) + \frac{N_t}{N_b}\theta''(\eta) = 0 \tag{14}$$

using the appropriate boundary condition as determined by Eqs. (5) and (6) in the form:

$$f(0) = 0, \ f'(0) = 1, \ \theta(0) = 1, \ \phi(0) = 1 \quad at \quad \eta = 0 \tag{15}$$

$$f'(\eta) = r, \ \theta(\eta) = 0, \ \phi(\eta) = 0 \quad at \quad \eta \to \infty \tag{16}$$

The Brownian motion parameter, thermophoresis parameter, thermal radiation parameter, Prandtl number, Hartmann number, porosity parameter, stagnation point parameter and the Lewis number are represented by the similarity parameters N_b, N_t, Nr, Pr, β, K, M, r and Le respectively in the equations mentioned above (12)-(16). They are defined as follows:

$$N_b = \frac{\Gamma D_B C_\infty}{\nu}, \ N_t = \frac{\Gamma D_T}{\nu T_\infty}(T_f - T_\infty), \ Nr = \frac{16}{3}\frac{\sigma^* T_\infty^3}{K^* K_f},$$
$$Pr = \frac{\nu}{\alpha}, \ \ M = \frac{\sigma B_0^2}{b\rho}, \ \ K = \frac{\nu}{bk_1}, \ r = \frac{a}{b}, \ \ Le = \frac{\alpha}{D_B} \tag{17}$$

Quantities like the rate of mass and heat transfer, as well as coefficient of friction factor, are interpreted as follows:

$$C_f = \frac{2\,\tau_w}{\rho u_w^2}, \ Nu_x = \frac{xq_w}{k_f(T_w - T_\infty)}, \ Sh_x = \frac{xq_m}{D_B(C_w - C_\infty)} \tag{18}$$

Where τ_w denote wall shear stress, surface heat flux is q_w and q_m shows mass flux.

$$\sqrt{Re_x}C_f = \left(1 + \frac{1}{\beta}\right)f''(0), \quad \frac{Nu_x}{\sqrt{Re_x}} = -(1 + Nr)\theta'(0),$$
$$\frac{Sh_x}{\sqrt{Re_x}} = -\phi'(0) \tag{19}$$

3. Solution Algorithm:

The bvp4c approach in MATLAB is applied to solve numerically the equations described above. Equations (12), (13), and (14) are transformed into first-order differential equations, and then solved while adhering to the specified boundary conditions (15)-(16) to interface with the bvp4c solver. The resulting the system of first-order differential equations, along with the transformed boundary conditions (20)-(28), is as follows:

$$f = y_1, \ f' = y_2, \ f'' = y_3, \ \ \theta = y_4, \ \theta' = y_5, \ \phi = y_6, \ \phi' = y_7 \tag{20}$$

Equations (10), (11), (12), (13) and (14) become

$$y_1' = y_2 \tag{21}$$

$$y_2' = y_3 \tag{22}$$

$$y_3' = \frac{1}{(1 + 1/\beta)}[y_2^2 - r^2 - y_1y_3 - (M + K)(r - y_2)] \tag{23}$$

$$y_4' = y_5 \tag{24}$$

$$y_5' = -\frac{Pr}{(1 + Nr)}[y_1y_5 + N_by_5y_7 + N_ty_5^2] \tag{25}$$

$$y_6' = y_7 \tag{26}$$

$$y_7' = -LePry_1y_7 + \frac{N_tP_r}{N_b(1 + Nr)}[y_1y_5 + N_by_5y_7 + N_ty_5^2] \tag{27}$$

The boundary condition yields

$$y_1(0) = 0, \ y_2(0) = 1, \ y_4(0) = 1, \ y_6(0) = 1 \quad at\ \eta \to 0$$

$$y_2(\eta) = r, \ y_4(\eta) = 0, \ y_6(\eta) = 0 \quad at\ \eta \to \infty \tag{28}$$

4. Results and discussion:

Under the boundary conditions (15) and (16), the reduced nonlinear ordinary differential equations (12)–(14) are numerically solved using the Bvp4c method. Several values of physical parameters are tested for this numerical solution. The impact of changing the governing parameters on the skin friction coefficient, concentration, temperature, dimensionless velocity, and local heat and mass transfer rates is investigated.

Table 1: Effect of various parameter on skin friction coefficient C_f

β	K	M	r	$f''(0)$	$(1+1/\beta)f''(0)$
0.5	0.6	1	0.5	- 0.5299	- 1.5897
1	0.6	1	0.5	- 0.6487	- 1.9461
1.5	0.6	1	0.5	- 0.7106	- 2.1318
2.0	0.6	1	0.5	- 0.7490	- 2.2470
1	0.5	1	0.5	- 0.6391	- 1.7042
1	1.0	1	0.5	- 0.6860	- 1.8293
1	1.5	1	0.5	- 0.7300	- 1.9466
1	2.0	1	0.5	- 0.7715	- 2.0573
1	0.6	0.5	0.5	- 0.5989	- 1.1978
1	0.6	1.0	0.5	- 0.6487	- 1.2974
1	0.6	1.5	0.5	- 0.6950	- 1.3900
1	0.6	2.0	0.5	- 0.7385	- 1.4770
1	0.6	1	0.1	- 1.0564	-2.1128
1	0.6	1	0.2	- 0.9647	- 1.9294
1	0.6	1	0.3	- 0.8660	- 1.7320
1	0.6	1	0.4	- 0.7606	- 1.5212

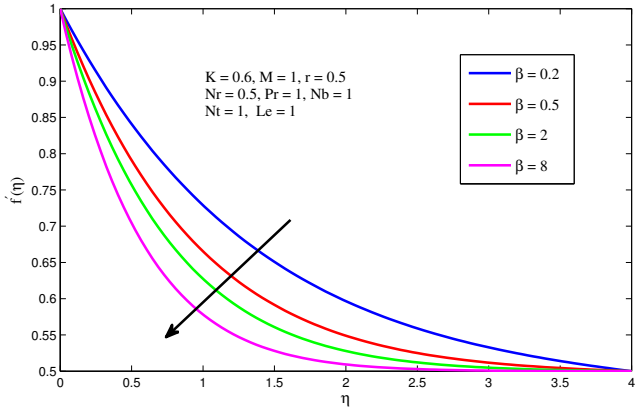

Figure 1: Influence of Casson fluid parameter on velocity of fluid.

The velocity graph's fluctuation in relation to the Casson parameter β is shown in Fig. 1. The graph indicates that thickness of velocity boundary layer reduces as values of β grow. This is because a rise in β causes a rise in plastic dynamic viscosity, which creates resistance to fluid flow and results in a drop in fluid velocity.

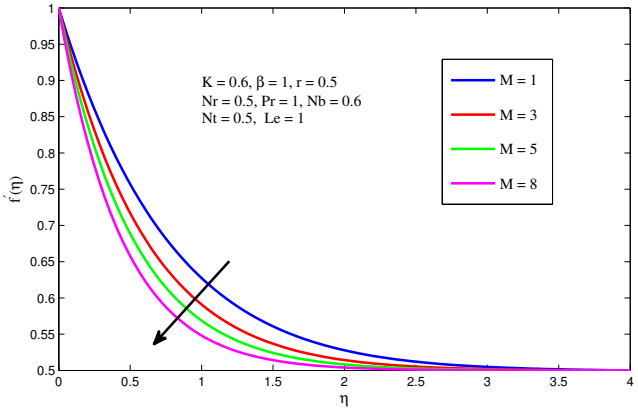

Figure 2: Influence of Mgnetic parameter on velocity of the fluid.

Figure 2 illustrates how raising the magnetic field parameter has negative impact on profile of velocity. The creation of the Lorentz force as a result of the rising magnetic field's strengthening of external electric field. In the opposite direction of the flow, the Lorentz force acts on the surface to lower velocity.

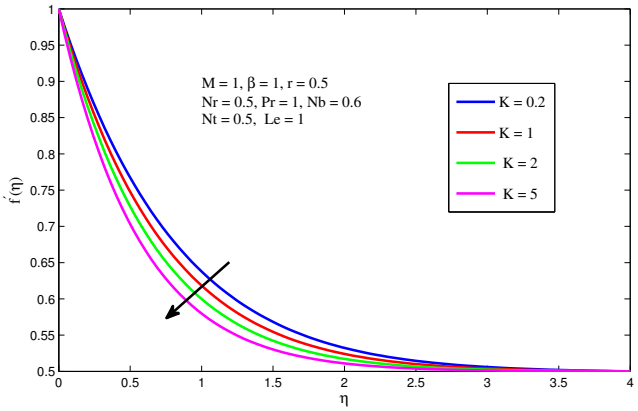

Figure 3: Influence of Porosity parameter on velocity of the fluid.

As illustrated in Fig. 3 the velocity profile decreases as porosity parameter varies. It indicates that as pores are bigger, the momentum of the flow through boundary layer gets less. Additionally, the existence of a permeable medium raises flow resistance, which lowers fluid motion and, as a result, lowers nanofluid velocity.

Table 2: The variation of Nusselt number (Nu_x) and Sherwood number (Sh_x) with respect to different parameters.

β	K	M	r	Nr	Pr	N_b	N_t	Le	$-(1+Nr)\theta'(0)$	$-\phi'(0)$
0.5	0.6	1	0.5	0.5	1	0.6	0.5	1	0.6461	0.6028
1	0.6	1	0.5	0.5	1	0.6	0.5	1	0.6284	0.5927
1.5	0.6	1	0.5	0.5	1	0.6	0.5	1	0.6230	0.5883
2.0	0.6	1	0.5	0.5	1	0.6	0.5	1	0.6200	0.5857
1	0.5	1	0.5	0.5	1	0.6	0.5	1	0.6292	0.5934
1	1.0	1	0.5	0.5	1	0.6	0.5	1	0.6254	0.5902
1	1.5	1	0.5	0.5	1	0.6	0.5	1	0.6219	0.5874
1	2.0	1	0.5	0.5	1	0.6	0.5	1	0.6188	0.5849
1	0.6	0.5	0.5	0.5	1	0.6	0.5	1	0.6326	0.5964
1	0.6	1.0	0.5	0.5	1	0.6	0.5	1	0.6284	0.5927
1	0.6	1.5	0.5	0.5	1	0.6	0.5	1	0.6246	0.5896
1	0.6	2.0	0.5	0.5	1	0.6	0.5	1	0.6212	0.5869
1	0.6	1	0.5	0.5	1	0.6	0.5	1	0.6284	0.5927
1	0.6	1	1.0	0.5	1	0.6	0.5	1	0.7278	0.6878
1	0.6	1	1.5	0.5	1	0.6	0.5	1	0.8139	0.7740
1	0.6	1	2.0	0.5	1	0.6	0.5	1	0.8904	0.8509
1	0.6	1	0.5	0.5	1	0.6	0.5	1	0.5892	0.5927
1	0.6	1	0.5	1.0	1	0.6	0.5	1	0.7340	0.6089
1	0.6	1	0.5	1.5	1	0.6	0.5	1	0.8710	0.6215
1	0.6	1	0.5	2.0	1	0.6	0.5	1	1.0038	0.6312
1	0.6	1	0.5	0.5	0.5	0.6	0.5	1	0.5481	0.4100
1	0.5	1	0.5	0.5	1.0	0.6	0.5	1	0.6284	0.5927
1	0.6	1	0.5	0.5	1.3	0.6	0.5	1	0.6457	0.7053
1	0.6	1	0.5	0.5	1.5	0.6	0.5	1	0.6472	0.7797
1	0.6	1	0.5	0.5	1	0.5	0.5	1	0.6544	0.5581
1	0.6	1	0.5	0.5	1	1.0	0.5	1	0.5323	0.6597
1	0.6	1	0.5	0.5	1	1.5	0.5	1	0.4291	0.6899
1	0.6	1	0.5	0.5	1	2.0	0.5	1	0.3430	0.7027
1	0.6	1	0.5	0.5	1	0.6	1.0	1	0.5536	0.5500
1	0.6	1	0.5	0.5	1	0.6	1.5	1	0.4881	0.5576
1	0.6	1	0.5	0.5	1	0.6	2.0	1	0.4305	0.6063
1	0.6	1	0.5	0.5	1	0.6	2.5	1	0.3798	0.6891
1	0.6	1	0.5	0.5	1	0.6	0.5	1	0.6633	0.3539
1	0.6	1	0.5	0.5	1	0.6	0.5	1	0.6284	0.5927
1	0.6	1	0.5	0.5	1	0.6	0.5	1	0.6078	0.7867
1	0.6	1	0.5	0.5	1	0.6	0.5	1	0.5945	0.9499

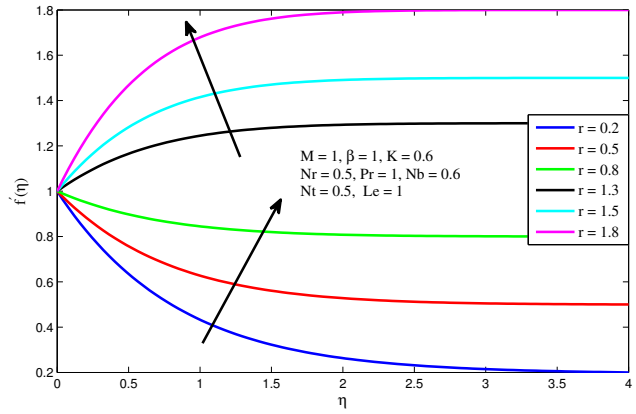

Figure 4: Influence of Stagnation point parameter on velocity of fluid.

The influence of the velocity ratio parameter r on the velocity plot can be observed in Figure 4. An increase in flow velocity occurs when free-stream velocity exceeds that of stretching sheet, or when r ≥ 1. However, the boundary layer thickness diminishes with higher values of r. Additionally, the velocity plot converges towards the velocity ratio parameter r as free-stream velocity surpasses stretching velocity. Conversely, a reduction in fluid velocity and hydrodynamic boundary layer thickness is noted when velocity of free-stream is smaller than that of the stretching sheet.

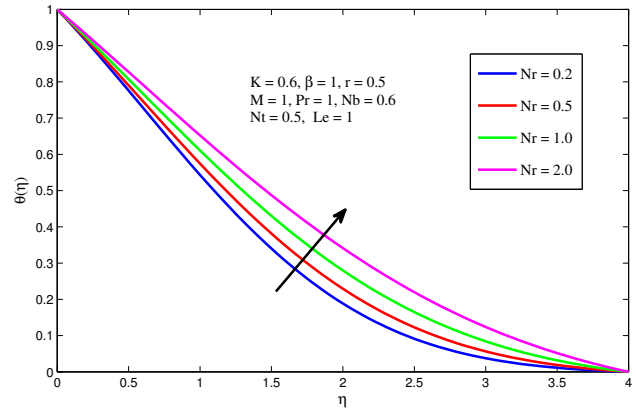

Figure 5: Influence of Radiation parameter on velocity of fluid.

The analysis of Fig. 5 shows that raising the value of Nr raises the temperature profile. The rate of heat transfer inside the boundary layer area is increased by a larger value of Nr because It increases the amount of heat that is transferred to the working fluid between the two layers.

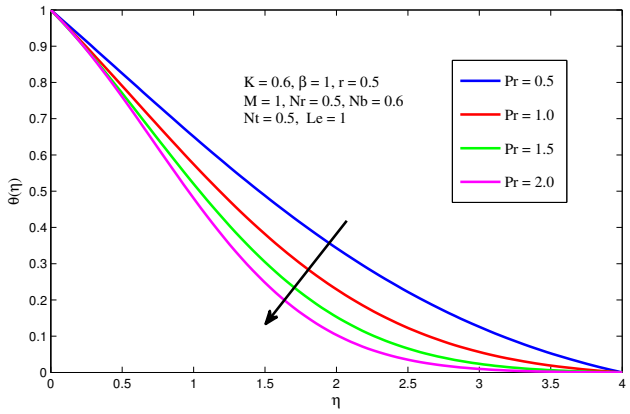

Figure 6: Effect of Prandtl number on temperature of fluid.

The temperature profile changes when the Prandtl number is applied, as seen in Fig. 6. The Prandtl number is the momentum diffusivity divided by the thermal diffusivity. A lower amount of thermal diffusivity is associated with an increase in Prandtl number. Therefore, the temperature drops due to a decrease in thermal diffusion.

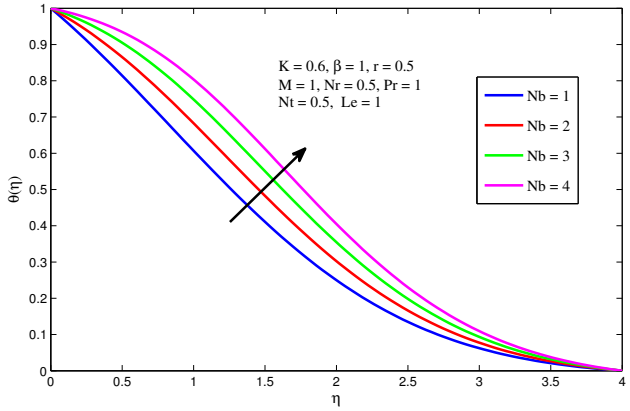

Figure 7: Influence of Brownian motion parameter on temperature of the fluid.

The influence of N_b on temperature profile is illustrated in Figure 7. It is evident that when N_b rises, mass diffusivity increases as well, raising the temperature within the boundary layer section.

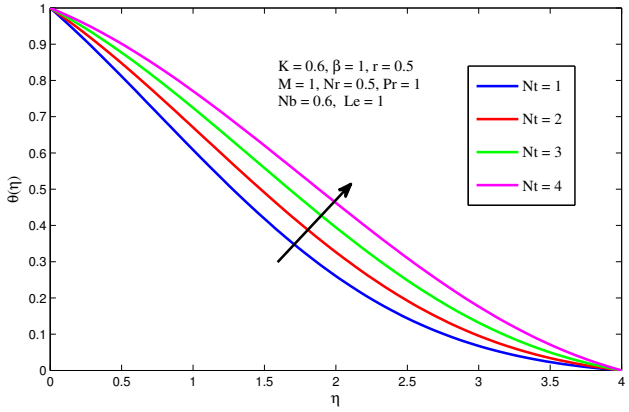

Figure 8: Influence of thermophoresis parameter on temperature of the fluid.

The plotted impacts of N_t on the profile of temperature is shown in Fig. 8. It is evident that when N_t rises, the temperature profile rises as well. It occurs as a result of the increased thermophoresis force caused by higher values of Nt, which has the propensity to transfer nanoparticles from hot surfaces to cold surfaces. Consequently, heat transmission rates for nanoparticles increase in the boundary layer area.

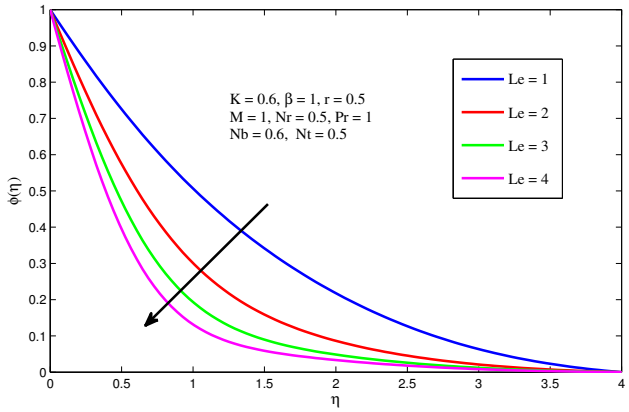

Figure 9: Influence of Lewis number on Concentration profile.

The Lewis number's impact on nanoparticle concentration profile is seen in Fig. 9. Higher values of *Le*, which is correlated with nanoparticle concentration and reduces mass concentration involving the nanoparticles and base fluid, are clear since the ratio of heat diffusivity to mass diffusivity is represented by the Lewis number. As a result, the value of *Le* increases and concentration profile of nanoparticles lowers.

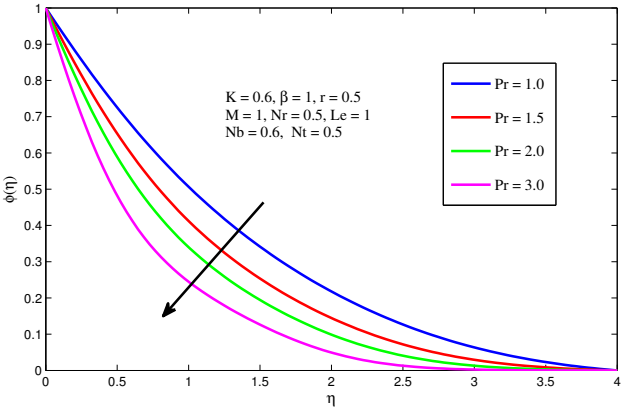

Figure 10: Influence of Prandtl number on Concentration profile.

Similar outcomes were shown in Figure 10 with the parameter *Pr*.

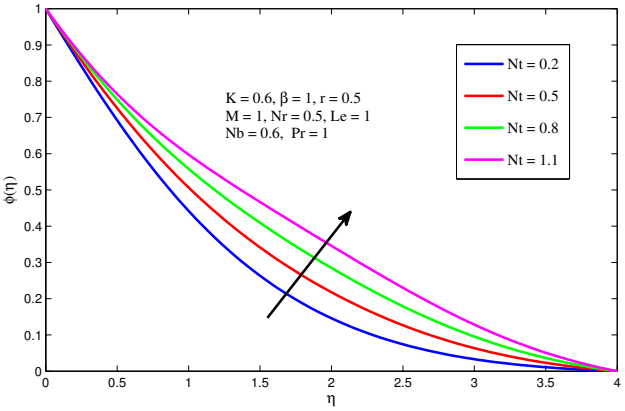

Figure 11: Influence of thermophoresis parameter on Concentration profile.

The effects of nanoparticle concentration with thermophoresis parameter N_t are shown in Fig. 11. It can be seen that value of N_t is followed by the nanoparticle concentration profile. It occurs as a result of increased thermophoresis force in boundary layer area caused by a greater value of N_t, which raises the concentration of nanoparticles.

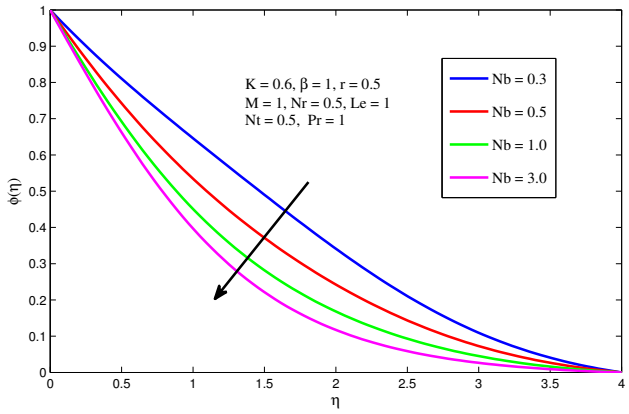

Figure 12: Influence of Brownian motion parameter on concentration profile.

Figure 12 shows $\phi(\eta)$ for various levels of N_b. It has been shown that as N_b grows, the thermal boundary layer's thermophoresis force decreases, which lowers the boundary layer's thickness concentration. when a result, when Nb grows, the nanoparticle concentration profile decreases.

5. Conclusion

In the present investigation, the examination delves into impacts of thermal radiation and magnetic field on flow of boundary layer at the stagnation point. This flow pertains to a scenario where it transpires across porous stretched sheet and encompasses a nanofluid characterized by Casson properties. The principal equations governing this flow phenomenon are converted into set of dimensionless differential equations, encompassing a variety of physical parameters. The boundary layer equations that govern the momentum and heat within the set are transformed into a series of ordinary differential equations through application of similarity transformations. Subsequently, the solution to these equations is derived utilizing the "bvp4c" function available within the MATLAB computational software package. This computational tool aids in the numerical solution of boundary value problems, providing a robust framework for analyzing the intricate interplay between thermal radiation, magnetic fields, and the flow characteristics at the stagnation point on the porous stretching sheet. The study's findings yield the following conclusions:

- A rise in the Prandtl number is associated with reduction in thermal diffusivity, resulting in a decline in temperature.
- The coefficient of skin friction is heightened by larger magnetic field parameters due to the decrease in velocity resulting from the generated Lorentz force. This decrease in velocity, in turn, leads to an increase in the drag force experienced at the surface.
- There is a drop in fluid velocity and hydrodynamic boundary layer thickness when the stretched sheet velocity is greater than the velocity of free-stream.
- The presence of a porous medium raises flow resistance, which lowers fluid motion and, as a result, lowers nanofluid velocity.
- An augmentation in thermal radiation parameter, Brownian motion parameter and thermophoresis parameter results in an augmentation in thermal boundary layer.
- This study has the potential to be applied in various areas, such as the enhancement of industrial processes like cooling systems and metal processing, the advancement of biomedical applications like drug delivery systems and the comprehension of blood flow, as well as the improvement of energy systems.

References

[1] K. Hiemenz, Die grenzschicht an einem in den gleichformigen flussigkeitsstrom eingetauchten geraden kreiszylinder, Dinglers Polytech. J. 326 (1911) 321–324.

[2] B. Sakiadis, Boundary-layer behavior on continuous solid surfaces: Ii. the boundary layer on a continuous flat surface, AiChE journal 7 (2) (1961) 221–225.

[3] F. Tsou, E. M. Sparrow, R. J. Goldstein, Flow and heat transfer in the boundary layer on a continuous moving surface, International Journal of Heat and Mass Transfer 10 (2) (1967) 219–235.

[4] H. A. Ghazwani, Unsteady mixed convective mhd boundary stagnation point nanofluid flow with multi-slip effects, variable wall temperature and porosity phenomenon, International Journal of Modern Physics B (2023) 2450089.

[5] A. Ali, H. S. Khan, S. Saleem, M. Hussan, Emhd nanofluid flow with radiation and variable heat flux effects along a slandering stretching sheet, Nanomaterials 12 (21) (2022) 3872.

[6] V. B. Awati, A. Goravar, et al., Semi-numerical investigation of boundary layer flow and heat transfer of magnetohydrodynamics nano-fluid flow in presence of chemical reaction over a non-isothermal porous medium, ASME Journal of Heat and Mass Transfer 145 (8) (2023).

[7] H. Waqas, H. Naeem, U. Manzoor, S. Sivasankaran, A. A. Alharbi, A. S. Alshomrani, T. Muhammad, Impact of electro-magneto-hydrodynamics in radiative flow of nanofluids between two rotating plates, Alexandria Engineering Journal 61 (12) (2022) 10307–10317.

[8] M. Kemparaju, B. Lavanya, M. M. Nandeppanavar, N. Raveendra, Casson mhd nano fluid flow with internal heat generation and viscous dissipation of an exponential stretching sheet., International Journal of Heat & Technology 40 (3) (2022).

[9] P. Thakur, A. Pargaonkar, S. S. Sonawane, Introduction to nanofluids, in: Nanofluid Applications for Advanced Thermal Solutions, Elsevier, 2023, pp. 1–19.

[10] H. Song, Y. Ye, Z. Zhang, S. Wang, T. Zhou, J. Guo, S. Zhang, A nanocleaning fluid for downhole casing cleaning, Polymers 15 (6) (2023) 1447.

[11] Y. Norasia, M. Tafrikan, B. H. Kamaluddin, Analysis of the magnetohydrodynamics nanoviscous fluid based on volume fraction and thermophysical properties, BAREKENG: Jurnal Ilmu Matematika dan Terapan 17 (1) (2023) 0331–0340.

[12] G. Vanitha, U. Mahabaleshwar, S. Bhattacharyya, Impact of thermal radiation on free-forced convective nanofluid flow due to a porous stretching/shrinking surface, in: Conference on Fluid Mechanics and Fluid Power, Springer, 2021, pp. 291–296.

[13] B. S. Goud, Y. D. Reddy, Numerical simulation of thermal radiation on an unsteady mhd nanofluid flow over an infinite vertical flat plate with ramped temperature, Special Topics & Reviews in Porous Media: An International Journal 14 (2) (2023).

[14] A. Asghar, L. A. Lund, Z. Shah, N. Vrinceanu, W. Deebani, M. Shutaywi, Effect of thermal radiation on three-dimensional magnetized rotating flow of a hybrid nanofluid, Nanomaterials 12 (9) (2022) 1566.

[15] B. K. Sharma, A. Kumar, R. Gandhi, M. M. Bhatti, N. K. Mishra, Entropy generation and thermal radiation analysis of emhd jeffrey nanofluid flow: Applications in solar energy, Nanomaterials 13 (3) (2023) 544.

[16] N. Vijay, K. Sharma, Entropy generation analysis in mhd hybrid nanofluid flow: Effect of thermal radiation and chemical reaction, Numerical Heat Transfer, Part B: Fundamentals (2023) 1–17.
[17] H. Yasmin, Z. Nisar, Mathematical analysis of mixed convective peristaltic flow for chemically reactive casson nanofluid, Mathematics 11 (12) (2023) 2673.
[18] M. Devi, U. Gupta, J. Sharma, Casson nanofluid instability with viscosity and conductivity variation using brinkman model, Journal of Nanofluids 12 (4) (2023) 955–966.
[19] M. Basit, M. Tahir, A. Riasat, S. Khan, M. Imran, A. Akgül, Numerical simulation of bioconvective casson nanofluid through an exponentially permeable stretching surface, International Journal of Modern Physics B (2023) 2450128.
[20] M. S. Arif, K. Abodayeh, Y. Nawaz, Design of finite difference method and neural network approach for casson nanofluid flow: A computational study, Axioms 12 (6) (2023) 527.
[21] M. S. Arif, K. Abodayeh, Y. Nawaz, Design of finite difference method and neural network approach for casson nanofluid flow: A computational study, Axioms 12 (6) (2023) 527.
[22] N. Kumar, K. S. Chaudhary, Neural network based fractional order sliding mode tracking control of nonholonomic mobile robots., Journal of Computational Analysis & Applications 33 (1) (2024).
[23] K. S. Chaudhary, N. Kumar, Fractional order fast terminal sliding mode control scheme for tracking control of robot manipulators, ISA transactions 142 (2023) 57–69.
[24] L. Mohan, A. Prakash, Stability and numerical analysis of the generalised time-fractional cattaneo model for heat conduction in porous media, The European Physical Journal Plus 138 (3) (2023) 1–28.
[25] A. Prakash, L. Mohan, Application of caputo fractional operator to analyse the fractional model of brain tumour via modified technique, International Journal of Applied and Computational Mathematics 9 (5) (2023) 117.
[26] L. Mohan, A. Prakash, Stability and numerical analysis of fractional bbm-burger equation and fractional diffusion-wave equation with caputo derivative, Optical and Quantum Electronics 56 (1) (2024) 26.
[27] L. Mohan, A. Prakash, Analysing the conduction of heat in porous medium via caputo fractional operator with sumudu transform., Journal of Computational Analysis & Applications 33 (1) (2024).
[28] L. Mohan, A. Prakash, Analysing the conduction of heat in porous medium via caputo fractional operator with sumudu transform., Journal of Computational Analysis & Applications 33 (1) (2024).
[29] L. Mohan, A. Prakash, Two efficient techniques for analysis and simulation of time-fractional tricomi equation, Sādhanā 49 (2) (2024) 1–13.
[30] P. Kumar, B. Singh, S. Goyal, K. Kumar, A. Nandan, K. S. Nisar, S. Alkhazaleh, A.-H. Abdel-Aty, Numerical solution of mhd micropolar casson fluid flow over porous linearly stretching sheet with heat source/sink, Appl. Math 18 (1) (2024) 183–190.
[31] S. Rosseland, Astrophysik: Auf atomtheoretischer grundlage (1931).